Compactifying fracton stabilizer models

Arpit Dua,[1,2] Dominic J. Williamson,[1] Jeongwan Haah,[3] and Meng Cheng[1]
[1]*Department of Physics, Yale University, New Haven, Connecticut 06520-8120, USA*
[2]*Yale Quantum Institute, Yale University, New Haven, Connecticut 06520, USA*
[3]*Quantum Architectures and Computation, Microsoft Research, Redmond, Washington 98052, USA*

(Received 9 April 2019; published 19 June 2019)

We investigate two-dimensional compactifications of three-dimensional fractonic stabilizer models. We find the two-dimensional topological phases produced as a function of compactification radius for the X-cube model and Haah's cubic code. Furthermore, we uncover translation symmetry enrichment in the compactified cubic code that leads to twisted boundary conditions.

DOI: 10.1103/PhysRevB.99.245135

I. INTRODUCTION

The exploration of topological order in three dimensions led to the surprising discovery of fracton models, whose topological excitations have emergent mobility restrictions [1–13]. A large class of these models can be realized by local commuting projector Hamiltonians and obey lattice definitions of topological order [14]. They are broken up into type-I [15–28] and type-II categories [29–32] depending on whether there are any string operators in the theory. Similar phenomena have been observed in higher rank gauge theories [33–50]. For a review of fracton lattice models and gauge theories, see Ref. [51].

In this work, we explore the properties of fracton models under compactification. Broadly speaking, compactification starts from a d-dimensional manifold of the form $M_{d-1} \times S^1$, and passes to the limit where the linear dimension of the $(d-1)$ manifold M_{d-1} is much larger than the size of the circle S^1. The d-dimensional theory is thus reduced to a $(d-1)$-dimensional one, which is oftentimes easier to analyze.

Previously, compactification has proven to be a very useful tool for understanding topological phases that fall into the framework of topological quantum field theory (TQFT) [52–63], in both two and three dimensions. In 3D, compactification reduces complicated loop excitations to more familiar pointlike anyons and allows for computation of the so-called three-loop braiding statistics of loop excitations [64–66]. In fact, many known (3+1)D TQFTs, including Abelian twisted Dijkgraaf-Witten gauge theories, can be completely classified according to their behavior under compactification [67]. In two dimensions, compactification was exploited in the classification of symmetry-enriched topological phases (SET) [68–70].

It is now widely recognized that fracton phases are sensitive to more than just topology, with their properties depending on certain geometric structures of the underlying manifold [71–79]. In this work, we only consider translation-invariant fracton models defined on regular cubic lattices. For the purpose of defining compactification, it is necessary to keep track of the length of the system in the compactified direction $\hat{z}$, which is well defined when there is translation symmetry along $\hat{z}$. We find that type-I and type-II fracton models behave very differently under compactification. In particular, we show that the fractal mobility constraint of type-II fractons is mapped onto the interplay between translation symmetries and topological order in the resulting (2+1)D model. This further provides a method to distinguish different type-II fracton models. For example, while Haah's cubic code and the renormalized cubic code B are closely related, as the latter was obtained from entanglement renormalization of the former, they are nevertheless distinct phases of matter [32], which is reflected in the difference between their translation actions. Surprisingly, we also find that the compactified models may exhibit subsystem symmetry-enriched topological order [80–84], leading to spurious contributions to their topological entanglement entropies [85–87].

The paper is laid out as follows: In Sec. II, we describe some general features of compactifying 3D stabilizer models; in Sec. III, we review the general structure of a compactified (3+1)D TQFT, giving the toric code as an example; in Sec. IV, we turn to the compactification of type-I fracton models, with a focus on the X-cube model; in Sec. V, we present the core results of the paper concerning compactification of type-II fracton models, focusing on Haah's cubic code; and finally we conclude in Sec. VI. In the Appendix, we present the data we have obtained by compactifying a large range of fracton stabilizer models.

II. COMPACTIFYING TOPOLOGICAL CODES

We begin with some general comments on compactifying topologically ordered lattice models.

Consider a 3D gapped lattice model defined on a spatial manifold $M_2 \times S^1$, where we take S^1 to be the $\hat{z}$ direction with periodic boundary condition. Taking the limit $L_x, L_y \to \infty$ while keeping L_z fixed to a finite value produces a 2D gapped lattice model. We follow the generally held belief that all 2D gapped spin lattice models are described by TQFTs and hence fall into stable phases labeled by an anyon model (modular tensor category) together with a consistent chiral central charge [88,89]. We also allow the

possibility of "unstable" phases that are direct sums of the stable phases that will instantaneously decohere into one of the constituents. Physically, this corresponds to some kind of spontaneous symmetry breaking. This happens whenever the 3D model supports nontrivial string operators that can wrap the $\hat{z}$ direction. In this case, the string operators wrapping the S^1 cycle become local operators in the 2D compactified model. Generally speaking, these operators can acquire finite expectation values, splitting the degeneracy between different sectors labeled by eigenvalues of the string operators. For models with zero correlation length (e.g., stabilizer codes), no such splitting occurs and the resulting ground space is a direct sum of all sectors.

For the infinite cubic lattice, our focus in this paper, we may specify an arbitrary lattice vector when we compactify a model. Hence, we may associate a function $n_{\vec{v}}^{\{s_i\}}$ to any lattice vector $\vec{v}$ and eigenvalues $\{s_i\}$ of the string operators that become local under compactification. This function takes values in the space of 2D topological phases.

A. Structure theorems for stabilizer codes

From here on, we focus on translation-invariant stabilizer Hamiltonians with topological order. These Hamiltonians are specified by a choice of local Pauli stabilizer generators $h^{(i)}$ which are given, up to a sign, by a tensor product of Pauli X, Y, and Z matrices, where

$$X = \begin{pmatrix} 0 & 1 \\ 1 & 0 \end{pmatrix}, \quad Y = \begin{pmatrix} 0 & -i \\ i & 0 \end{pmatrix}, \quad Z = \begin{pmatrix} 1 & 0 \\ 0 & -1 \end{pmatrix}. \quad (1)$$

The stabilizer generators become the interaction terms

$$H = \sum_{\vec{v}} \left(\mathbb{1} - h_{\vec{v}}^{(i)}\right), \quad (2)$$

where $h_{\vec{v}}^{(i)}$ indicates a local generator $h^{(i)}$ after translation by a lattice vector $\vec{v}$; in fact, we can loosen this translation invariance by including a $\vec{v}$-dependent sign factor. We require the Hamiltonian to consist of commuting terms, be frustration free, and satisfy the topological order condition defined in Ref. [31]. We say that a stabilizer Hamiltonian is CSS [93,94] if each generator $h^{(i)}$ consists exclusively of either Pauli X or Z terms.

Starting with a translation-invariant 3D topological stabilizer Hamiltonian, we can compactify it along a lattice vector $\vec{v}$ and fix the eigenvalues $\{s_i\}$ of any string operators that become local. This leaves us with a translation-invariant (up to signs) 2D topological stabilizer Hamiltonian. We can then rely on the existing rigorous classification of such models [90,92] represented in Fig. 1 which ensures that they are equivalent, up to a locality preserving Clifford unitary circuit, to a finite number of copies of the 2D toric code [95] and some trivial product state. If the stabilizer Hamiltonian is CSS, a Clifford local unitary suffices [91]. This implies that, after fixing out any local degeneracy, the complete topological phase-invariant $n_{\vec{v}}^{\{s_i\}}$ for a compactified 3D topological stabilizer model is simply the number of copies of 2D toric code it is equivalent to.

There is a similar structure theorem for 1D stabilizer models [31] that is useful for calculating the compactification

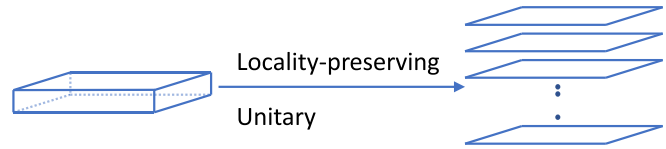

FIG. 1. Structure theorem [90–92]: a translation invariant topological stabilizer Hamiltonian in 2D is equivalent to copies of toric code and a trivial state via a locality-preserving unitary. This can be used to decompose a compactified 3D model (left) into copies of the 2D toric code (right).

of a 2D stabilizer Hamiltonian. This structure theorem states that any translation-invariant 1D stabilizer model is equivalent to copies of the 1D quantum Ising model and some trivial product state.

B. Calculating the 2D topological order

We now outline how to analyze the 2D stabilizer models obtained via compactification. For the remainder of the paper, we consider compactifying along a spatial axis, usually chosen to be $\hat{z}$. Technically, we pass from 3D to 2D by grouping all the qubits along a single column in the $\hat{z}$ direction, which is being compactified, onto a single lattice site. Thus, a 3D model with Q qubits per site is mapped to a 2D model with QL_z qubits per site, where L_z is the compactification radius. Next, we fix the eigenvalue of any string operators wrapping the $\hat{z}$ direction by adding a term proportional to them to the Hamiltonian. By the structure theorem, we know that this 2D stabilizer code is equivalent to a number $n_{L_z}^{\{s_i\}}$ of toric codes. Hence, we can find a basis of $2n_{L_z}^{\{s_i\}}$ anyonic excitations that generate all others via fusion. These anyons appear at the ends of $2n_{L_z}^{\{s_i\}}$ string operators that can be organized into anticommuting pairs. The commutation matrix of these string operators, defined below, determines the S matrix invariant of the relevant topological phase [96,97]. Half the rank of the commutation matrix is equal to the number of toric codes and hence in this case it is a complete invariant. It furthermore does not suffer from spurious contributions, due to subsystem symmetries, which may afflict attempts to extract the number of copies of toric code from a topological entanglement entropy calculation [87].

To calculate the number of anticommuting string operator pairs in a 2D stabilizer model we consider two overlapping striplike subregions of the 2D lattice, one horizontal and one vertical, as shown in Fig. 2. We search for Pauli string operators in these subregions that may only create excitations at their end points. These are included in the kernel of the excitation map with closed boundary conditions along the length of the strips, and open boundary conditions at the ends, where closed boundary conditions correspond to including stabilizer generators that cross the boundary, and open boundary conditions do not.

We label the generating set of Pauli string operators found on the horizontal (vertical) strip by S_i^h, $i = 1, \ldots, N$ (S_j^v, $j = 1, \ldots, N'$). However, many of these strings may create trivial anyons, i.e., in the vacuum sector. To address this, we construct the commutation matrix C, which is defined

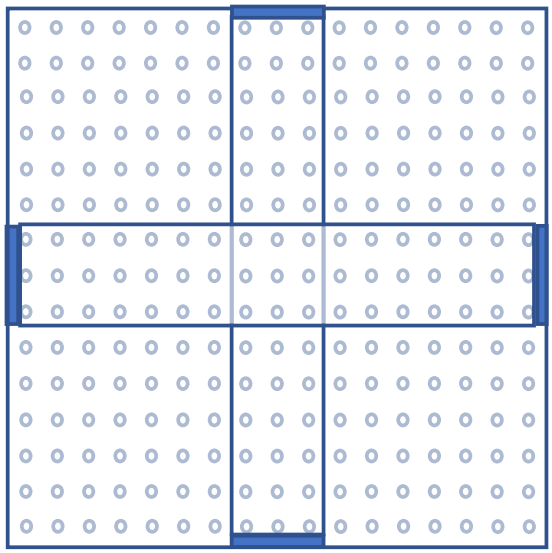

FIG. 2. A section of a 2D stabilizer model is shown, with circles depicting the qubits. Two strips are shown, with solid blue bars on the ends denoting open boundary conditions and thin lines denoting closed boundary conditions. Half the rank of the commutation matrix between operators on the strips gives the number of copies of toric code.

elementwise by

$$C_{i,j} = \begin{cases} 0 & \text{if } \left[S_i^h, S_j^v\right] = 0\,, \\ 1 & \text{if } \left[S_i^h, S_j^v\right] \neq 0\,. \end{cases} \tag{3}$$

The $\mathbb{Z}_2$ rank of C is the number of independent pairs of anticommuting string operators. For these string operators to anticommute the anyons, they create must be nontrivial. Hence, half of the rank gives the number of copies of 2D toric code equivalent to the model, as each copy contributes two independent string operator generators. Therefore, if the 2D stabilizer model has been obtained from a compactification specified by L_z, $\{s_i\}$, we have

$$n_{L_z}^{\{s_i\}} = \tfrac{1}{2}\text{rank } C\,. \tag{4}$$

C. Calculating the action of translation

Calculating the action of translation upon the anyons requires more detailed information about the topological order. We first isolate a basis of string operators that move a generating set of anyons from those that create topologically trivial excitations. This is achieved by bringing the commutation matrix into Smith normal form

$$UCV = D\,, \tag{5}$$

where U and V are invertible (unimodular) matrices and D is the Smith normal form, which is diagonal. Since we are working over $\mathbb{Z}_2$, the nonzero entries of D consist of rank C entries of 1 along the diagonal. Hence, we can truncate U to its first rank C rows, call this $\bar{U}$, and V to its first rank C columns, call this $\bar{V}$, and we have

$$\bar{U}C\bar{V} = \mathbb{1}_{\text{rank } C}\,. \tag{6}$$

The rows of $\bar{U}$ specify products of string operators S_i^h that give a basis for the horizontal strip: $\bar{S}_i^h$, $i = 1, \ldots,$ rank C. Similarly, the columns of $\bar{V}$ specify a conjugate basis for the vertical strip: $\bar{S}_j^v$, $j = 1, \ldots,$ rank C, satisfying

$$\left[\bar{S}_i^h, \bar{S}_j^v\right] = \begin{cases} 0 & \text{if } i \neq j\,, \\ 2\bar{S}_i^h\bar{S}_j^v & \text{if } i = j\,. \end{cases} \tag{7}$$

For CSS code models, we can treat the Pauli X and Z strings separately and this ensures that the string operators in our basis move self-bosonic anyons. We have done so for all the CSS code examples considered in this work.

The string operator basis we have found allows us to calculate the action of translation in the horizontal direction by simply shifting the vertical string operators over one site, $T_x^{-1}\bar{S}_j^v T_x$, and similarly for the vertical translations $T_y^{-1}\bar{S}_i^h T_y$. This is because we can use the modularity of anyon braiding to identify the shifted vertical strings with the original basis via their commutation relations with the unshifted horizontal strings. To implement this, we form a new commutation matrix given by

$$(C_x)_{i,j} = \begin{cases} 0 & \text{if } \left[\bar{S}_i^h, T_x^{-1}\bar{S}_j^v T_x\right] = 0\,, \\ 1 & \text{if } \left[\bar{S}_i^h, T_x^{-1}\bar{S}_j^v T_x\right] \neq 0\,. \end{cases} \tag{8}$$

Taking the Smith decomposition, we find

$$U_x C_x V_x = \mathbb{1} = C_x V_x U_x\,, \tag{9}$$

and hence the change of basis matrix for the vertical strings, $V_x U_x$, gives the generator of the translation action, $\bar{T}_x$, on the anyons. Similar reasoning yields $\bar{T}_y = V_y U_y$.

The action of translation on the anyons is fully specified by $\bar{T}_x$ and $\bar{T}_y$ in the examples we have considered. This is because these matrices describe the permutation of anyons by translation, and no symmetry fractionalization occurs in the examples considered. However, it can be hard to interpret these matrices directly. In the examples below, we have focused on a simple invariant of the translation action: O_i, the order of the permutation. That is, the smallest nonzero solution to $\bar{T}_i^{O_i} = \mathbb{1}$. These orders give the dimensions of the smallest unit cell $O_x \times O_y$ one must take such that the coarse-grained translation does not permute anyons. Moreover, for an $L_x \times L_y$ system with periodic boundary conditions, if an O_i does not divide L_i the boundary conditions will be twisted. This leads to a reduction in the ground-state degeneracy, compared to the untwisted value $4^{n_{L_z}^{\{s_i\}}}$.

Under compactification, the remaining 3D translation symmetry along the $\hat{z}$ direction is mapped to a $\mathbb{Z}_{L_z}$ on-site permutation symmetry. Following the method above, we can work out the action $\bar{T}_z$ of this symmetry on the anyons in the resulting 2D model and derive properties such as its order O_z.

III. COMPACTIFICATION OF TQFTS

In this section, we review the compactification of 3D topological phases that are described by TQFTs. It is generally believed, on physical grounds, that TQFTs in (3+1)D support two types of excitations at low energy: particles and loops, both of which are mobile. These excitations can be created and moved by appropriate topological string and membrane

operators, which can be locally deformed as long as their boundary is kept fixed. By definition, topological invariance ensures that the compactified (2+1)D theory will also be a TQFT and that all choices of compactification direction and radius lead to the same theory. The resulting (2+1)D theory will generally not be stable but will correspond to a *cat state* consisting of an unstable sum of multiple different stable TQFTs. This is due to topologically nontrivial string operators wrapping the compactified direction, which become local operators in the compactified theory. We expect (under a modularity assumption) that such compactified string operators can be used to project onto a definite flux, or string, excitation threading the compactified S^1. Topologically nontrivial membrane operators on a plane orthogonal to the compactified direction become global symmetries of the resulting (2+1)D model, and the compactified string operators split the symmetry-breaking degeneracy. On the other hand, membrane operators wrapping the compactification direction become string operators for flux loops wrapping the compactified direction, which are mapped to pointlike particles. Hence, the topological order after compactification is given by

$$\mathrm{TO}_{3\mathrm{D}}^{\mathrm{comp}} \cong \bigoplus_{s} \mathrm{TO}_{2\mathrm{D}}^{\{s\}}. \tag{10}$$

where $\{s\}$ denotes the eigenvalues of the string operators. Assuming the original set of string excitations and dual string operators was complete, each of the resulting 2D theories should be stable. Hence, $n_{\vec{v}}^{\{s\}} = \mathrm{TO}_{2\mathrm{D}}^{\{s\}}$ for arbitrary $\vec{v}$.

In the most general setting, it can be quite difficult to calculate the resulting (2+1)D topological orders $\mathrm{TO}_{2\mathrm{D}}^{\{s\}}$. However, the answer is known for all twisted Dijkgraaf-Witten theories [52] (twisted quantum double models). This reduction has proven useful for the calculation of many properties of (3+1)D TQFTs, including the classification of loop defects, and the computation of three-loop braiding statistics, and generalizations thereof, which completely classify Abelian Dijkgraaf-Witten theories [64–67].

A. The 2D toric code

As a warmup, we consider compactifying the 2D toric code. This example captures many of the essential features of compactifying a TQFT and is relevant for the type-I example to follow.

The 2D Toric code model is commonly defined with one qubit per edge of a square lattice. Here, we group a pair of qubits from orthogonal, adjacent edges onto each site. The local stabilizer generators in the Hamiltonian are then given by

$$\begin{array}{ccc} ZI - II & & XI \quad XX \\ | \quad\quad | & & | \quad\quad | \\ ZZ - IZ & & II - IX \end{array}. \tag{11}$$

The logical operators on a torus are given by anticommuting pairs of string operators $\bar{X}_{\hat{\imath}}, \bar{Z}_{\hat{\jmath}}$, where $\hat{\imath} \neq \hat{\jmath} \in \{\hat{x}, \hat{y}\}$. One pair of representative logical operators is given by

$$\bar{X}_{\hat{x}} = \prod_{x} IX_{(x,0)}\,, \quad \bar{Z}_{\hat{y}} = \prod_{y} IZ_{(0,y)}\,, \tag{12}$$

and the other is defined similarly.

Under compactification along the $\hat{y}$ direction, we obtain two copies of the 1D quantum Ising model, up to local unitary.

To see this, we make use of the structure theorem in one dimension which states that any translation invariant 1D stabilizer model is equivalent to copies of the 1D quantum Ising model and some trivial product state. This reduces the problem to counting the number of local-nonlocal pairs of logical operators in the compactified model. Since the compactification of 2D toric code along one direction maps two out of the four logical string operators to local logical operators, the topological ground-space degeneracy reduces to an unstable symmetry-breaking degeneracy. The remaining two logical operators map to global spin-flip symmetries for two copies of the Ising model and this is consistent with the fourfold ground-state degeneracy of the 2D toric code.

B. The 3D toric code

For the next example, we consider the 3D toric code. Similar to the 2D toric code, we have grouped three qubits onto each lattice site, and the stabilizer generators are given by

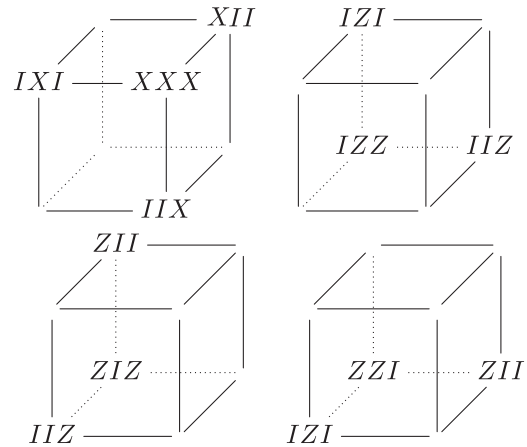

. (13)

Representative logical operators on a torus are generated by three anticommuting membrane-string operator pairs $\bar{X}_{\hat{\imath}}, \bar{Z}_{\hat{\imath}}$, where $\hat{\imath} = \hat{x}, \hat{y}, \hat{z}$. A representative pair is given by

$$\bar{X}_{\hat{x}} = \prod_{y,z} XII_{(0,y,z)}, \quad \bar{Z}_{\hat{x}} = \prod_{x} ZII_{(x,0,0)}\,, \tag{14}$$

and similarly for $\hat{y}$ and $\hat{z}$.

Compactifying the $\hat{z}$ direction makes $\bar{Z}_{\hat{z}}$ into a local logical operator that anticommutes with a global symmetry given by $\bar{X}_{\hat{z}}$. The compactification further maps $\bar{X}_{\hat{x}}, \bar{X}_{\hat{y}}$ into nontrivial string operators, while $\bar{Z}_{\hat{x}}, \bar{Z}_{\hat{y}}$ remain nontrivial string operators, and their commutation relations are preserved. Moreover, these generate all the logical operators, up to stabilizers. To make a precise identification with copies of toric code, we need to be slightly more careful and study the superselection sectors. We find a basis of two inequivalent superselection sectors for a fixed eigenvalue of $\bar{Z}_{\hat{z}}$. These are represented by a compactified string excitation that consists of Z-stabilizer violations wrapping the $\hat{\hat{z}}$ direction and a single X-stabilizer violation. This, combined with the anticommutation of the aforementioned string operators that move these anyons, identifies the resulting (2+1)D phase as equivalent to a direct sum

of two toric codes,

$$\mathrm{TC}_{3\mathrm{D}}^{\mathrm{comp}} \cong \mathrm{TC}_{2\mathrm{D}} \oplus \mathrm{TC}_{2\mathrm{D}}\,. \tag{15}$$

For this example, and the 2D example above, translation acts trivially.

IV. COMPACTIFICATION OF TYPE-I FRACTON MODELS

In this section, we consider the compactification of type-I fracton models, treating the X-cube model as a prototypical example. According to their definition [7], type-I fracton models feature some completely immobile pointlike excitations (i.e., fractons) alongside other excitations that are mobile in one or more directions. This includes lineons, which can move only in one direction, and planons, which can move in two directions. Moreover, the fractons should not be composites of mobile excitations that can move in different directions. In type-I models, there can be an extensive number of inequivalent string operators in the direction of compactification that, after being mapped to local operators, lead to an extensive number of symmetry-breaking sectors.

A. X-cube model

The stabilizer generators for the X-cube model [7] are given by

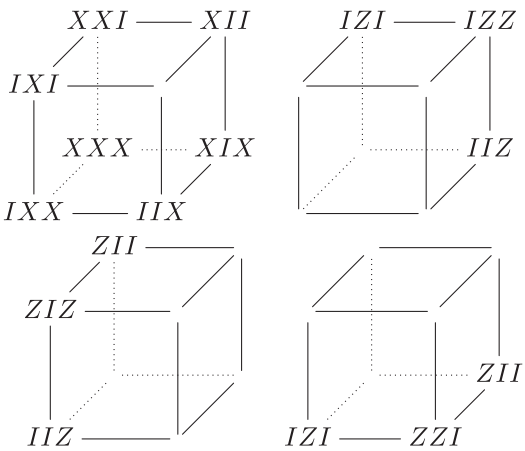

. (16)

Here, we have grouped three qubits onto each vertex, similar to the 3D toric code example. We consider this model on an $L_x \times L_y \times L_z$ cuboid with periodic boundary conditions. To enumerate the logical operators, let us first define anticommuting pairs $\bar{X}^{\hat{i}}_{\hat{k},\ell}, \bar{Z}^{\hat{j}}_{\hat{k},\ell}$, where $\hat{i} \neq \hat{j} \neq \hat{k} \in \{\hat{x}, \hat{y}, \hat{z}\}$ and $\ell = 0, \ldots, L_k - 1$, along intersecting pairs of noncontractible loops as follows,

$$\bar{X}^{\hat{x}}_{\hat{z},\ell} = \prod_x XII_{(x,0,\ell)}, \quad \bar{Z}^{\hat{y}}_{\hat{z},\ell} = \prod_y ZII_{(0,y,\ell)}\,, \tag{17}$$

and similarly for other permutations of $\hat{x}, \hat{y}, \hat{z}$. This set of operators is overcomplete due to the relations

$$\prod_\ell \bar{X}^{\hat{i}}_{\hat{k},\ell} = \prod_\ell \bar{X}^{\hat{k}}_{\hat{i},\ell}, \quad \bar{Z}^{\hat{i}}_{\hat{j},0} = \bar{Z}^{\hat{i}}_{\hat{k},0}\,. \tag{18}$$

Removing $\bar{X}^{\hat{x}}_{\hat{z},0}, \bar{X}^{\hat{y}}_{\hat{z},0}, \bar{X}^{\hat{y}}_{\hat{x},0}, \bar{Z}^{\hat{x}}_{\hat{z},0}, \bar{Z}^{\hat{y}}_{\hat{z},0}, \bar{Z}^{\hat{z}}_{\hat{x},0}$, and replacing

$$\bar{Z}^{\hat{x}}_{\hat{z},\ell} \mapsto \bar{Z}^{\hat{x}}_{\hat{z},0}\bar{Z}^{\hat{x}}_{\hat{z},\ell}, \quad \bar{Z}^{\hat{y}}_{\hat{z},\ell} \mapsto \bar{Z}^{\hat{y}}_{\hat{z},0}\bar{Z}^{\hat{y}}_{\hat{z},\ell}, \tag{19}$$

where $\ell > 0$, and

$$\bar{X}^{\hat{x}}_{\hat{y},0} \mapsto \bar{X}^{\hat{x}}_{\hat{y},0} \prod_{i=1}^{L_x} \bar{X}^{\hat{y}}_{\hat{x},i}\,, \tag{20}$$

we arrive at a complete set of $(2L_x + 2L_y + 2L_z - 3)$ logical operator pairs. We remark that this basis has been chosen such that the $2(L_z - 1)$ logical operator pairs with a $\hat{z}$ subscript are deformable in the xy plane.

Under compactification along the $\hat{z}$ direction, all logical operators with a $\hat{z}$ superscript become local. Hence, $(L_x + L_y - 1)$ logical $\bar{Z}$ operators become local, while their anticommuting $\bar{X}$ partners are mapped to rigid subsystem symmetries. Similarly, $(L_x + L_y)$ logical $\bar{X}$ operators become local, while their anticommuting logical $\bar{Z}$ partners become linear subsystem symmetries. After fixing out the extensive, local degeneracy due to subsystem symmetry breaking, by fixing eigenvalues $\{s_i\}$ of the logical operators with a $\hat{z}$ superscript, we are left with $(2L_z - 2)$ logical operator pairs that are deformable in 2D. These correspond to the string operators of $(L_z - 1)$ copies of toric code wrapping the torus. Hence, each symmetry-breaking sector of the compactified X-cube model is local-unitary equivalent to $(L_z - 1)$ copies of toric code, where L_z is the compactification radius. That is,

$$n_{L_z}^{\{s_i\}} = \mathrm{TC}_{2\mathrm{D}}^{\otimes(L_z-1)}\,. \tag{21}$$

We have verified these facts numerically using the anticommuting string operator calculation explained in Sec. II.

In this case, the translations $\bar{T}_x, \bar{T}_y$, act trivially on the copies of toric code but nontrivially on the symmetry-breaking sectors. On the other hand, $\bar{T}_z$ acts nontrivially on both the copies of toric code and the symmetry-breaking sectors.

The results of this compactification provide several signatures that differentiate the X-cube model from a decoupled stack of 2D toric code layers. The clearest signature is in the constant correction -1 to the number of toric codes occurring as L_z is increased. This constant correction, as shown above, is reflected in the subsystem symmetry breaking under compactification. It is also consistent with the fact that one can disentangle a copy of 2D toric code from two layers of the X-cube model via a local unitary [75]. In fact, for each lattice direction of compactification, one gets a -1 constant correction and hence is related to the total -3 correction in the number of logical operator pairs in the 3D model. From the 2D toric code example in Sec. III, we also see that the pattern of subsystem symmetry breaking in the compactified X cube is subtly different than that occurring in compactified layers of 2D toric code. It would be interesting to use similar signatures from compactification to identify and classify nontrivial type-I models in the future.

V. COMPACTIFICATION OF TYPE-II FRACTON MODELS

In this section, we turn our attention to type-II fracton models, focusing on the canonical example: the cubic code. By their definition [7], type-II fracton models do not have any string operators, and thus *all* nontrivial particle excitations are immobile. In such models, isolated excitations can be created at the corners of fractal operators. For example, in the cubic

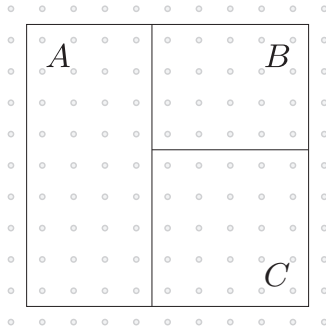

FIG. 3. Regions used to calculate the topological entanglement entropy.

code [2], a fractal operator exists with support on a Sierpinski tetrahedron.

Since there are no string operators in a type-II model, no local logical operators can occur after compactification. Hence, the resulting 2D models will be topologically ordered. The compactification of a translation-invariant type-II stabilizer model in the $\hat{z}$ direction is then simply characterized by the number of toric codes it is equivalent to as a function of length, n_{L_z}.

The quantity n_{L_z} has to be calculated on a model-to-model basis, but it does satisfy a simple bound that depends upon the locality of the stabilizer generators. Let's consider compactification of a type-II stabilizer model where the support of each stabilizer generator is a single cube. One can show that the number of copies of Toric code as a function of compactification radius L_z is upper bounded i.e. $n_{L_z} \leqslant 2L_z$. This is achieved by considering the topological entanglement entropy (TEE) computed via the Kitaev-Preskill prescription of tripartite information $I(A, B, C)$, given by

$$S_A + S_B + S_C - S_{AB} - S_{BC} - S_{AC} + S_{ABC}\,,$$

on the regions shown in Fig. 3. More generally for any 2D translation-invariant topological stabilizer model, with Q qubits per site and Q independent generators per plaquette which only act on the sites at the corners, we have $n_{L_z} \leqslant Q$. In fact, when there are no relations among the generators, and the plaquette stabilizers generated by them act nontrivially on all corners, then we find the value of $I(A, B, C)$ to be saturated, i.e., $Q = -I(A, B, C)$. One would expect this to determine n_{L_z}, as it was argued in Ref. [98] that $n_{L_z} = -I(A, B, C)$. However, it has recently been realized [85–87] that spurious contributions to the TEE may cause $n_{L_z} \leqslant -I(A, B, C)$. We find that this behavior occurs for the cubic code example below. For this reason, we use the more careful approach described in Sec. II to calculate n_{L_z} accurately.

The anyons in a compactified type-II model descend from immobile fracton excitations in 3D, raising the following question: How does the fractonic immobility manifest in the 2D compactified model? We find that the immobility is reflected in the 2D model as a nontrivial enrichment of the topological order by on-site and translation symmetries. These symmetries descend from the translation symmetries of the 3D model in the $\hat{z}$, and $\hat{x}, \hat{y}$ directions, respectively. The immobility of fractons in 3D implies that translates of a nontrivial excitation are topologically distinct and therefore a pair of such excitations cannot be created by a string operator. In other words, the action of translation symmetry must change the topological superselection sectors of the fracton excitations. Descending to 2D, via compactification, this implies that translations permute the anyon types. In contrast to the 3D type-II model, the action of translation on its 2D compactification must have a finite order [99]. This can be understood as originating from some operators in 3D that wrap around the compactified direction and pairwise create a nontrivial topological excitation and some translate of it. Such an operator would not exist purely in the 3D bulk without the compactified boundary condition. For example, let O_x denote the order of $\bar{T}_x$ in the compactified model, and then some string operator in 2D can create any excitation along with its translation by $T_x^{O_x}$. We remark that for CSS codes the action of translation is restricted to permuting excitations of the X stabilizers among themselves, and similarly for the Z stabilizers.

A. Cubic code

The main example we consider is the cubic code, which is known to be a type-II stabilizer model [2], i.e., it has no string operators and all nontrivial excitations are immobile. The generators of the stabilizer group are given by

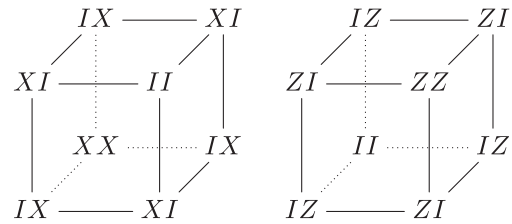

(22)

and their translations. See Fig. 4 for the patterns of excitations that are created on the dual cubic lattice by local operators. The remainder of this section focuses on the compactification of the above model.

1. Compactified topological order

We consider a family of 2D models produced by compactifying the cubic code, following the procedure in Sec. II. By the structure theorem presented there, the compactified cubic code models are unitarily equivalent to some number n_{L_z} copies of toric code. We have numerically calculated n_{L_z} for a range of values L_z by finding pairs of anticommuting string operators as explained in Sec. II. These results are presented in Table I.

The numerical scaling of n_{L_z} fits a simple formula for $L_z = 2^i \ell$, where $2 \nmid \ell$, given by

$$n_{L_z} = \begin{cases} 2L_z & \text{if } 3 \nmid L_z\,, \\ 2L_z - 2^{i+2} & \text{if } 3 \mid L_z\,. \end{cases} \tag{23}$$

In the next subsection, we prove that the above formula in fact holds for all L_z explicitly, using the framework of polynomial rings [5]. This scaling is substantially simpler than the scaling of the ground-space degeneracy of the cubic code on an $L \times L \times L$ 3D torus [31]. One may then ask the following: How is it possible that the ground-space degeneracy of n_{L_z} copies of toric code on an $L_x \times L_y$ torus matches the ground-space degeneracy of the cubic code on an $L_x \times L_y \times L_z$ 3D torus? The

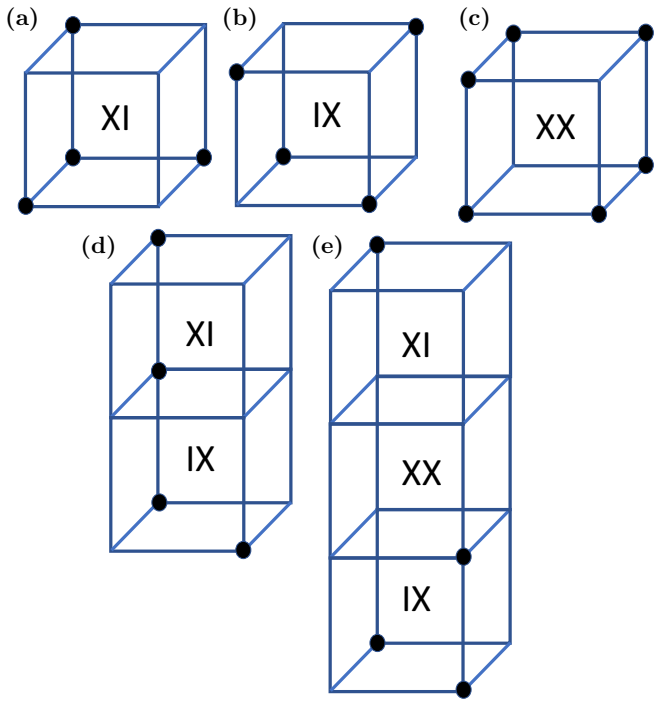

FIG. 4. Excitation patterns of stabilizers located on the vertices of the dual cubic lattice, which are created by local operators on pairs of qubits inside each cube: (a) XI, (b) IX, (c) XX, (d) IX–XI along $\hat{z}$, and (e) IX–XX–XI along $\hat{z}$.

TABLE I. As a function of compactification radius L_z we list: $R/2$ half the rank of the commutation matrix C, which equals the number of copies of toric code n_{L_z}, for the compactified cubic code. The order $O_x = O_y$ is the order of the translation actions $\bar{T}_x$, $\bar{T}_y$. The order O_z is the order of the on-site symmetry $\bar{T}_z$.

L_z	$n_{L_z} = R/2$	$O_x = O_y$	O_z
1	2	2	1
2	4	4	2
3	2	2	1
4	8	8	4
5	10	30	5
6	4	4	2
7	14	126	7
8	16	16	8
9	14	126	9
10	20	60	10
11	22	682	11
12	8	8	4
13	26	2730	13
14	28	252	14
15	26	30	15
16	32	32	16
17	34	510	17
18	28	252	18
19	38	19418	19
20	40	120	20
21	38	126	21
22	44	1364	22

answer lies in the nontrivial action of translation symmetry on the n_{L_z} toric codes contained in the compactified cubic code. Further details are given in the following subsections.

To build intuition for the scaling of n_{L_z}, we first notice that an adjacent pair of plaquettes, each having $2L_z$ stabilizers, can support 2^{4L_z} excitations, including vacuum. If these excitations are all topologically distinct, i.e., there are no nontrivial string operators confined to the pair of plaquettes, then the pair of plaquettes can support all the charge sectors of $2L_z$ copies of toric code. If we suppose that the pair of plaquettes still support all sectors when they also support nontrivial string operators, we can find the topologically inequivalent sectors by modding out the relations introduced by those string operators.

The simplest case with $n_{L_z} \leqslant 2L_z$ occurs when $n_3 = 2$, which was studied in detail in Ref. [87]. To provide an explanation, we direct the reader's attention to Fig. 4(e), which shows an excitation pattern created by a local operator. For compactified boundary conditions with $L_z = 3$, the operator in Fig. 4(e) allows an excitation to hop between stabilizers related by a $\hat{z}$ translation. Modding out by these relations, we find 2^4 inequivalent sectors on the pair of plaquettes. Furthermore, under compactifed boundary conditions, combining the operators in Fig. 4(e) with Figs. 4(a) and both 4(a) and 4(b), we find two diagonal hopping operators for each type of excitation on any plaquette. Hence, we find a model equivalent to two copies of toric code with $\bar{T}_x$, $\bar{T}_y$ acting as layer swap and $\bar{T}_z$ acting trivially. This agrees with the numerical results.

More generally, whenever $3|L_z$, one can find string operators on a column by taking products of operators similar to that shown in Fig. 4(e). For $2 \nmid L_z$, there are again two independent string operators on each plaquette for each type of stabilizer. Because of the bifurcating real-space renormalization group flow of the cubic code demonstrated in Ref. [32], the number of toric codes n_{L_z} doubles as we double L_z, i.e., $n_{2L_z} = 2n_{L_z}$, which accounts for the value of n_{L_z} in the remaining cases of Eq. (23) in which $2|L_z$.

2. *Copies of toric code from the polynomial framework*

In this subsection, we compute the number of copies of the 2D toric codes in the cubic code compactified in the z direction by a periodic boundary condition of linear size L_z. We employ the framework of polynomial rings developed in Ref. [5], but for the sake of brevity we do not introduce the formalism here. The no-strings rule of the cubic code implies that the compactified code is exact. By the classification theorem of exact CSS codes, the number n_{L_z} of embedded toric codes is half the dimension of the torsion submodule of cokerϵ [91, V.13]. Therefore, our starting point is the formula

$$n_{L_z} = \dim_{\mathbb{F}_2} \frac{\mathbb{F}_2[x^{\pm}, y^{\pm}, z^{\pm}]}{\left(1 + x + y + z, 1 + xy + yz + zx, z_z^L + 1\right)}. \tag{24}$$

As always, we lift the coefficient field to its algebraic closure $\mathbb{F} \supset \mathbb{F}_2$. The ring in this equation has a finite $\mathbb{F}$ dimension. So, it is isomorphic to the finite direct sum of localizations at maximal ideals $(x - a - 1, y - b - 1, z - t - 1)$, where

$a, b, t \in \mathbb{F} \setminus \{1\}$ are arbitrary; the constant 1 is inserted for convenience in notation later.

Put $L = 2^i \ell$ where ℓ is odd. In order for the localized ring not to vanish, the constants a, b, t has to be chosen to "satisfy" the ideal. In particular, $a + b + t = 0$, $ab + bt + ta = 0$, and $(1 + t)^\ell + 1 = 0$. So, $a = \omega t$ and $b = \omega^2 t$ where ω is either one of the two third roots of unity. Since $a, b, t \neq 1$, the constant t is further restricted so that $t \neq 1, \omega, \omega^2$. Put $\mathfrak{m} = (u - a, v - b)$, where $a \neq 1$, $b \neq 1$ and $a + b = t \neq 1$. We can make substitutions $x \to u + 1, y \to v + 1, z \to 1 + x + y = 1 + u + v$ so that

$$n_{L_z} = \sum_{\mathfrak{m}} \dim_{\mathbb{F}} \mathbb{F}[u, v]_{\mathfrak{m}}/\mathfrak{J}_{\mathfrak{m}}$$

where

$$\begin{aligned}\mathfrak{J}_{\mathfrak{m}} &= (u^2 + uv + v^2, (1 + u + v)^L + 1)_{\mathfrak{m}} \\ &= \left(u^2 + uv + v^2, u^{2^i} + v^{2^i} + t^{2^i}\right)_{\mathfrak{m}} \\ &= \left(u^2 + uv + v^2, uv^{2^i - 1} + (n + 1)v^{2^i} + t^{2^i}\right)_{\mathfrak{m}}. \end{aligned} \quad (25)$$

The second line follows from the first because the equation $z^{L_z} + 1$ factorizes into linear factors raised to power 2^i, but the localization at $\mathfrak{m}$ singles out only one factor. The third line uses $u^{2^i} = uv^{2^i - 1} + iv^{2^i} \mod u^2 + uv + v^2$ for any integer $i \geqslant 0$.

Suppose $t \neq 0$. Then, $\mathfrak{J}_{\mathfrak{m}}$ is equal to $(u - \omega^2 v, (\omega^2 + 1 + i)v^{2^i} + t^{2^i})_{\mathfrak{m}}$, so such $\mathfrak{m}$ contributes to the sum by 2^i. If ℓ is not a multiple of 3, then there are $2(\ell - 1)$ such $\mathfrak{m}$. If ℓ is a multiple of 3, then there are $2(\ell - 3)$ such $\mathfrak{m}$ because we have to exclude the third roots of unity.

Suppose $t = 0$. Then, $a = b = 0$, i.e., $\mathfrak{m} = (u, v)$. Then,

$$\mathfrak{J}_{\mathfrak{m}} = \left(u^2 + uv + v^2, uv^{2^i - 1} + (i + 1)v^{2^i}\right)_{(u,v)}.$$

Regardless of whether i is even or odd, one can show that $\{u^2 + uv + v^2, uv^{2^i - 1} + (i + 1)v^{2^i}, v^{2^i + 1}\}$ is a Gröbner basis for $\mathfrak{J}$ in the degree term order. We see that $(2^i + 1) + (2^i - 1) = 2^{i+1}$ contributes to the sum.

Therefore,

$$n_{L_z} = \begin{cases} 2^i 2(\ell - 1) + 2^{i+1} = 2L_z & \text{if } 3 \not| L_z, \\ 2^i 2(\ell - 3) + 2^{i+1} = 2L_z - 2^{i+2} & \text{if } 3 \,|L_z. \end{cases} \quad (26)$$

3. Translation symmetry enrichment

As alluded to above, the immobility of the topological sectors in the cubic code is reflected in the symmetry-enriched topological order of the compactified models. The relevant symmetries are the translations: T_x, T_y, and T_z which are mapped to translation and on-site symmetries under compactification, respectively. The nontrivial action of the translation symmetries on the compactified models leads to symmetry-twisted boundary conditions that remarkably allow the ground-space degeneracy of n_{L_z} copies of toric code on an $L_x \times L_y$ torus to match the ground-space degeneracy of the cubic code on an $L_x \times L_y \times L_z$ 3D torus.

The action of T_x, T_y, and T_z on the anyons in compactified cubic code takes the form of a permutation that does not mix e excitations of the X stabilizers with m excitations of the Z stabilizers. In fact, because of symmetries of the cubic code Hamiltonian, we find that the action of the translation symmetries simplifies further. The symmetry of reflection across the $\hat{x} \pm \hat{y}$ planes implies T_x and T_y act on the anyons in an isomorphic way. The further symmetry given by a combined spatial inversion, on-site swap, and Hadamard, implies that the action of any T_i on the e sector is isomorphic to the same T_i symmetry acting on the m sector. Hence, we focus our attention on the action of T_x and T_z on the e sector. These actions are specified by $n_{L_z} \times n_{L_z}$ binary matrices $\bar{T}_x$ and $\bar{T}_z$ that describe the action of T_x and T_z on the basis of e string operators found using the approach covered in Sec. II.

While we have explicitly calculated the matrices $\bar{T}_x$ and $\bar{T}_z$ for $L_z \leqslant 22$, they are only unique up to a change of basis for the anyons and are not enlightening when presented in raw form. For this reason, we focus on an important gauge-invariant quantity of the symmetry-enriched topological phase: the orders $O_x = O_y$ and O_z of the translation actions within the automorphism group of the anyons; see Sec. II. The values of O_i are tabulated in Table I.

The orders of permutation in the $\hat{x}$ and $\hat{y}$ directions have a clear physical interpretation: $O_x \times O_y$ is the minimal coarse-grained unit cell for which translation symmetries $T_x^{O_x}, T_y^{O_y}$ act trivially on the anyons. In other words, on a torus with $O_x \not| L_x$ or $O_y \not| L_y$ the boundary conditions are twisted by a nontrivial translation action. For n_{L_z} copies of toric code on an $L_x \times L_y$ torus with twisted boundary conditions, i.e., at least one of $L_x \mod O_x$ or $L_y \mod O_y$ are nonzero, the ground-state degeneracy is reduced to $< 4^{n_{L_z}}$. In fact the ground-space degeneracy is known to be given by the number of $T_x^{L_x}$-symmetric $T_y^{L_y}$ defects, or vice versa [99]. Hence, the complicated behavior of the cubic code's ground-space degeneracy on a 3D torus can be understood via the symmetry-enriched topological order of the compactified model.

Observe in Table I that the order of translation O_x is doubled as the compactification radius L_z is doubled. This, in fact, holds in general, which we will proceed to prove. To achieve this, we make use of the following formula for $\log_2$ of the ground-space degeneracy of the cubic code on an $L_1 \times L_2 \times L_3$ torus [31]

$$d = \begin{cases} 2^{l_1 + 1} d_1 - 1 & \text{if } l_1 = l_2, \\ 2^{l_1 + 1} d_1 & \text{otherwise.} \end{cases} \quad (27)$$

In the above, without loss of generality, $l_1 \leqslant l_2 \leqslant l_3$ indicates the number of factors of 2 in the prime factorizations of L_1, L_2, L_3, and

$$\begin{aligned} d_1 = \deg_x \gcd((1 + x)^{\ell_1} + 1, (1 + \omega x)^{\ell_2} + 1, \\ (1 + \omega^2 x)^{\ell_3} + 1)_{\mathbb{F}}, \end{aligned} \quad (28)$$

where $\ell_i = 2^{-l_i} L_i$, $1 + \omega + \omega^2 = 0$ and $\mathbb{F}$ is the algebraic closure of $\mathbb{F}_2$. In particular, if $L_1 = L_2 = L_3$ then $l_1 = l_2$.

Proposition 1. For any value $L_z = 2^{l_z} \ell_z$, consider $O := O_x = O_y = 2^o O'$, where $2 \not| \ell_z, O'$. Then, $o - l_z = 1$.

Proof. The proof is by contradiction: First, let us assume $o = l_z$. If we change the length of the periodic 2D lattice directions from $L_x = L_y = O$, which implies $l_x = l_y = l_z = o$, to $L_x' = L_y' = 2^i O$ for any natural number i, which implies $l_z = o < l_x' = l_y' = o + i$, the degeneracy must change from

$2^{o+1}d_1 - 1$ to $2^{o+1}d_1$. Since the value of d_1 does not depend on l_x, l_y, l_z, the degeneracy has decreased upon multiplying L_x, L_y by 2^i. However, the degeneracy should be maximal, and constant, for all untwisted boundary conditions $L_x = L_y = nO$, with n being a natural number. Hence, $o \neq l_z$.

Next, let us assume $o - l_z < 0$. Then, similarly going from $L_x = L_y = O$ with $l_x = l_y = o < l_z$ to $L_x{}' = L_y{}' = 2^{l_z - o+1}O$ with $l_z < l_x' = l_y' = l_z + 1$ changes the degeneracy from $2^{o+1}d_1 - 1$ to $2^{l_z+1}d_1$. However, for L_x' and L_y' being any positive integer multiples of the order O, the ground-state degeneracy should not change. Thus, $o - l_z < 0$ is not consistent.

Finally, let us assume $o - l_z \geqslant 2$. If we change lengths from $L_x = L_y = O$ to $L_x{}' = L_y{}' = 2^{-i}O$, for $0 < i < o - l_z$ we go from $l_z < l_x = l_y = o$ to $l_z < l_x' = l_y' = o - i$, while for $i \geqslant o - l_z$ we go to $l_x' = l_y' = o - i \leqslant l_z$. Thus, for $0 < i < o - l_z$, the degeneracy does not change. This is not consistent with O being the order of a nontrivial anyon permuting translation action. To see this, note that $L_x', L_y' < O$ corresponds to twisted boundary conditions that must lead to a strictly smaller ground-space degeneracy than the maximal value for $L_x = L_y = O$.

The only consistent possibility remaining is $o - l_z = 1$. ■

Next, we argue that the order of the translation action doubles upon doubling the compactification radius, $O(2L_z) = 2O(L_z)$. Consider compactifying the cubic code with radius L_z; the smallest torus corresponding to untwisted boundary conditions is given by $L_x = L_y = O(L_z)$ which leads to a degeneracy $4^{n_{L_z}}$. Doubling the compactification radius to $2L_z$, we have shown above that $n_{2L_z} = 2n_{L_z}$. Then periodic boundary conditions $L_x = L_y = 2O(L_z)$ lead to the maximal possible degeneracy $4^{2n_{L_z}}$ and hence correspond to untwisted boundary conditions. Therefore, $2O(L_z) = kO(2L_z)$ for a natural number k, and the above lemma implies $2 \nmid k$. Furthermore, we find that the ground-space degeneracy for compactification radius L_z and $L_x = L_y = O(L_z)/k$ is again maximal, $4^{n_{L_z}}$. This implies $k = 1$, or else there would be a contradiction with $O(L_z)$ being the order of a nontrivial translation action.

Proposition 2. Suppose $L_z = 2^i\ell$ with ℓ odd. Then, we have $O_x = O_y \leqslant 2^{i+1}(2^k - 1)$ where k is the least common multiple of 2 and the multiplicative order of 2 modulo L_z. In particular,

$$O_x \leqslant 2^{i+1}(2^{\ell-1} - 1), \tag{29}$$

$$O_x = 2^{i+1}\ell \quad \text{if } \ell = 2^n - 1 \text{ for } n \text{ even}, \tag{30}$$

$$O_x \leqslant 2^{i+1}\ell(\ell + 2) \quad \text{if } \ell = 2^n - 1 \text{ for } n \text{ odd}. \tag{31}$$

We also have $O_z = L_z$ if $\ell \neq 3$ and $O_z = 2^i$ if $\ell = 3$.

Proof. For the above proposition, it suffices to assume $i = 0$. We use the polynomial method [100] and Galois theory [101]. Recall that the charge module for the compactified cubic code is $\mathbb{F}_2[x^{\pm}, y^{\pm}, z]/J$, where $J = (1 + x + y + z, 1 + xy + yz + zx, z^\ell - 1)$. The translation group acts as the monomial multiplication. As noted earlier, $O_x = O_y$ from the symmetry $x \leftrightarrow y$. The order O_x is the minimum positive integer such that $x^{O_x} - 1 \in J$. We estimate the order O_x by considering the zeros of the ideal J. The first two generators of J defines a variety of codimension 2, and the compactification condition $z^L - 1$ selects finitely many points in this variety. Specifically, the first two generators define two lines that are parametrized as $(\omega^2 + \omega t, \omega + \omega^2 t, t)$ and $(\omega + \omega^2 t, \omega^2 + \omega t, t)$, where t is arbitrary, and $\omega \in \mathbb{F}_4$ is a third root of unity satisfying $\omega^2 + \omega + 1 = 0$. The polynomial $z^\ell - 1$ is separable (no degenerate roots), and the variety will be rational over the minimal extension field $\mathbb{F}_{2^k}$ over $\mathbb{F}_2$ that contains all the ℓth root of unity, which form a cyclic group $\mathbb{Z}/\ell\mathbb{Z}$, and ω. Every nonzero element of $\mathbb{F}_{2^k}$ is a root of $x^{2^k-1} - 1$, a power of which must belong to J. Localizing at the points of the two lines, we see that $(x^{2^k-1} - 1)^2 \in J$. (Localization at (1,1,1) shows that $x = 1$ has twofold degeneracy.) Thus, the order O_x is at most $2(2^k - 1)$. It remains to compute k for inequalities.

Since any automorphism of E over $\mathbb{F}_2$ should send a generator ζ of the group of all Lth root of unity to another generator, the splitting field $\mathbb{F}_2(\zeta)$ of $z^\ell - 1$ has at most $|(\mathbb{Z}/\ell\mathbb{Z})^\times| = \varphi(\ell)$ automorphisms over $\mathbb{F}_2$. In fact, since the automorphism of a finite field of characteristic 2 is always a composition of Frobenius map $\gamma \mapsto \gamma^2$, the group $\mathrm{Aut}(\mathbb{F}_2(\zeta)/\mathbb{F}_2)$ has order k' that is equal to the multiplicative order of 2 modulo ℓ. By Artin's theorem, we see the extension degree $[\mathbb{F}_2(\zeta) : \mathbb{F}_2]$ equals k', which divides $\varphi(\ell) \leqslant \ell - 1$. If k' is even, then $\mathbb{F}_2(\zeta)$ already contains ω (since ω has degree-2 minimal polynomial), and we have $k' = k \leqslant \ell - 1$. If k' is odd, then $\mathbb{F}_2(\zeta)$ does not contain ω and we have $k = 2k'$. Since $L - 1$ is even, in any case we have $k|(\ell - 1)$. If $\ell + 1 = 2^n$, then the multiplicative order of 2 modulo ℓ is n. This proves all the inequalities.

Furthermore, if $\ell + 1 = 2^n$ with n even, then the x coordinate of the two lines ranges over exactly all the nonzero elements of $\mathbb{F}_{2^n}$, and we see $x^m - 1 \in \mathrm{rad}J$ if and only if m is a multiple of n. This proves the lower bound in this special case and hence the equality.

To compute O_z, we again look at the two lines. Since we have to avoid $x = 0$ or $y = 0$ planes as the variables x and y are invertible, the parameter t is not equal to any of $\omega, \omega, 0$, but otherwise any value is allowed.

Localizing at maximal ideals $\mathfrak{m} = (x - a, y - b, z - c)$, where $(a, b, c) \neq (1, 1, 1)$, we immediately see that $J_\mathfrak{m}$ contains $(z - c)^m$ for $m = 2^i$ but not for $0 \leqslant m < 2^i$, The same is true for $\mathfrak{m} = (x - 1, y - 1, z - 1)$ thanks to the Gröbner basis computation that we have performed in the course of computing n_{L_z} above. The "multiplicity" of any z coordinate is 2^i.

If 3 does not divide ℓ, then $0, \omega^{\pm}$ are not roots of $z^\ell - 1$, and so $z^m - 1 \in \mathrm{rad}J$ for $m = \ell$ but not for $m < \ell$. By the multiplicity of the previous paragraph, $O_z = L_z$. If 3 divides ℓ, then $z^2 + z + 1$ divides $z^\ell - 1$ and the z coordinates take values precisely among the roots of $f(z) = (z^\ell - 1)/(z^2 + z + 1)$. By the multiplicity, $f(z)^{2^i} \in J$ and any smaller power than 2^i will invalidate the membership. It remains to find the minimum $m \geqslant 0$ such that $f(z)^{2^i}|(z^m - 1)$. Let $m = 2^j m'$ with m' odd. For the multiplicity, we know $j \geqslant i$ and $f(z)|(z^{m'} - 1)$. The degree of $f(z)$ is $\ell - 2$ which must be $\leqslant m'$, so minimum m' is one of $\ell - 2, \ell - 1, \ell$. If $\ell = 3$, then $m' = 1$ is the minimum. If $\ell > 3$, then a root of $f(z)$ is a primitive ℓth root of unity which can be a root of $z^{m'} - 1$ only if $m' = \ell$. ■

4. Translation defects

As mentioned above, the degeneracy due to twisted boundary conditions on an $L_x \times L_y$ torus is equal to the number of $T_x^{L_x}$-symmetric $T_y^{L_y}$ defects and vice versa [99]. By combining Eq. (23) with the degeneracy formula in Eq. (27) and Lemma 1, we can compute a large range of ground-state degeneracies and hence numbers of symmetric defects. Fix a compactification radius L_z, and for $L_x = L_y = O$ we have $d_1 = 2^{-l_z} n_{L_z}$. The degeneracy 2^d for $L_x = O/2^i$, $L_y = O/2^j$ specifies the number of $T_x^{O/2^i}$-symmetric $T_y^{O/2^j}$ defects as follows:

$$d = \begin{cases} 2^{l_z+1} d_1 - 1 & \text{for } i = 0,\ j = 1, \\ 2^{l_z+2-i} d_1 - 1 & \text{for } i = j > 0, \\ 2^{l_z+2-i} d_1 & \text{for } i > j > 0, \\ 2^{l_z+2-j} d_1 & \text{for } j > i \geqslant 0,\ j > 1. \end{cases} \tag{32}$$

Since the compactified models are equivalent to copies of toric code, they only support Abelian anyons. Hence, all the $T_x^{L_x}$ translation defects have the same quantum dimension, as they are related by fusion with the anyons. We recall that the total quantum dimension of any defect sector is equal to that of the anyons [99]. This implies that the number of $T_x^{L_x}$ defects, N_{L_x}, is related to their common quantum dimension, δ_{L_x}, via $N_{L_x} \delta_{L_x}^2 = 4^{n_{L_z}}$. Since $\log_2 N_{L_x} = d$, where d is $\log_2$ of the ground-space degeneracy of the cubic code on an $L_x \times O(L_z) \times L_z$ 3D torus, we have $\log_2 \delta_{L_x} = n_{L_z} - d/2$.

Since N_{L_x} is the same as the number of anyon types that are symmetric under a translation $T_x^{L_x}$, we can compute it directly from the dimension of the invariant subspace under $\bar{T}_x^{L_x}$. In particular, we have computed the number of unit translation T_x defects in this way for the values of L_z listed in Table I:

$$\log_2 N_1 = \begin{cases} 4 & \text{for } 2 \,|L_z, \\ 2 & \text{for } 2 \not| L_z. \end{cases} \tag{33}$$

Hence, the quantum dimensions δ_1 fit the following formula as a function of L_z:

$$\log_2 \delta_1 = \begin{cases} n_{L_z} - 2 & \text{for } 2 \,|L_z, \\ n_{L_z} - 1 & \text{for } 2 \not| L_z. \end{cases} \tag{34}$$

Our above results for N_1 imply that changing the periodic boundary conditions of the cubic code slightly, from $O(L_z) \times O(L_z) \times L_z$ to $[O(L_z) + 1] \times O(L_z) \times L_z$, can result in an extensive jump of the ground-space degeneracy, from $4^{n_{L_z}}$ to N_1. This provides an appealing interpretation for the seemingly erratic behavior of the ground-space degeneracy of the cubic code on periodic boundary conditions in terms of the better understood phenomena of translation symmetry twisted boundary conditions of a 2D topological order.

B. Cubic code B

Our second example is cubic code B [32], which is specified by the following generators:

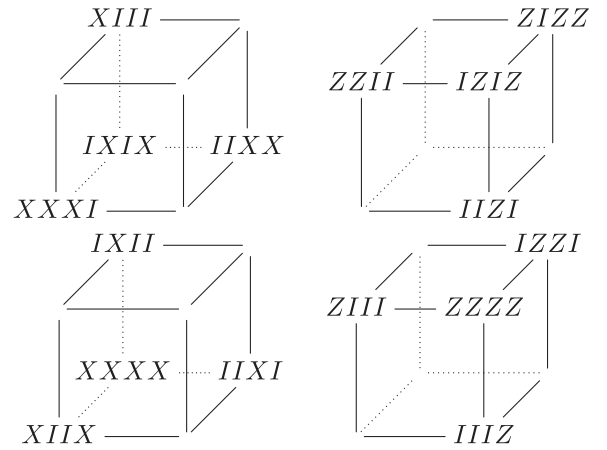

(35)

This model was found from bifurcation of the original cubic code under real-space entanglement-renormalization and hence is also type II. More specifically, a local unitary circuit U was found which is invariant under a coarse-grained translation group, generated by T_x^2, T_y^2, T_z^2, and satisfies

$$U H_A(a) U^\dagger \cong H_A(2a) + H_B(2a)\,. \tag{36}$$

In the above, $H_A(a)$ denotes the original cubic code A Hamiltonian with lattice spacing a, $H_B(2a)$ denotes the B cubic code Hamiltonian with lattice spacing $2a$, and $\cong$ denotes that the stabilizer group of two Hamiltonians is the same, up to tensoring with ancilla qubits in the product state $|0\rangle^{\otimes N}$. We remark that the equivalence $\cong$ does not imply that the stabilizer generators on the left and right strictly match after the removal of ancillas.

Cubic code B was further found to be self-bifurcating. That is, under another local unitary circuit V, which respects the coarse-grained translation group generated by T_x^2, T_y^2, T_z^2, Ref. [32] found

$$V H_B(a) V^\dagger \cong H_B(2a) + H_B'(2a)\,. \tag{37}$$

For the compactification of cubic code B along the $\hat{z}$ direction, we have found

$$\begin{aligned} n_{L_z}^B &= n_{L_z}^A\,, \\ O^B(L_z) &= O^A(L_z)/2\,, \\ \log_2 N_1^B &= 4\,. \end{aligned} \tag{38}$$

Hence, the cubic codes A and B lead to the same topological phase under compactification. However, this does not imply the original models lie in the same topological phase. On the other hand, the translation symmetry-enriched phases after compactification are different, but this is not yet sufficient to show that the original models lie in different phases. This is because one is allowed an arbitrary, finite coarse-graining step when comparing the original models. An obvious first step is to coarse grain the $\hat{x}$ and $\hat{y}$ directions of cubic code A by a

factor of 2, to ensure the order of the translation actions match. After this transformation, the symmetry-enriched topological orders resulting from the compactification of cubic codes A and B are still distinct. To see this, we consider the number of unit translation defects for the compactified coarse-grained A code, which equals the number of T_x^2 translation defects for the original compactified A code,

$$\log N_2^A = \begin{cases} 8 & \text{for } 4 \mid L_z, \\ 6 & \text{for } 2 \mid L_z,\ 4 \nmid L_z, \\ 4 & \text{for } 2 \nmid L_z. \end{cases} \tag{39}$$

No coarse graining in the $\hat{z}$ direction can bring this into agreement with N_1^B. However, this is still only a necessary condition for the original cubic codes A and B to lie in distinct phases.

It was shown in Ref. [32] that it is impossible to find any coarse grainings of cubic codes A and B that make their ground-space degeneracies agree for periodic boundary conditions on all system sizes. Hence, they are distinct topological phases of matter. From the point of view of compactification, this implies that no coarse grainings can be made such that cubic code A and B lead to the same symmetry-enriched topological orders for all compactifications. In particular, since the ground-space degeneracies cannot always be made to match, even after an arbitrary coarse graining the number of symmetric defects of all types in the compactified models cannot be made to match.

VI. DISCUSSION AND CONCLUSIONS

In this work, we have studied compactifications of translation-invariant stabilizer models with fracton topological order. We found that type-I fracton order is reflected by a combination of topological order and symmetry breaking in the compactified model that has a simple scaling with the compactification radius. More interestingly, we found that type-II fracton order manifests in the symmetry-enriched topological order of the compactified model. The topological order has a relatively simple scaling with the compactification radius but is enriched in a complicated way by translation symmetry. We have analytically and numerically studied various aspects of the compactification in detail for the 2D and 3D toric code, X-cube model, and the cubic code. Our results on the cubic code provide an understanding of the model's complicated ground-space degeneracy in terms of twisted boundary conditions for copies of the 2D toric code enriched by translation symmetry. In fact, such translation symmetry enrichment can be also be found for type-1 models like Yoshida's model [4] under compactification. Along this direction of the string operator, translation action is trivial and varying the system size along it does not change the ground-space degeneracy.

More generally, our results draw a connection between fracton topological phases in 3D and translation symmetry-enriched topological phases in 2D which may prove useful for their classification.

Furthermore, we encountered nontrivial subsystem symmetry-enriched phases in our study of the compactified cubic code, which led to spurious contributions to the topological entanglement entropy [98,102]; see Ref. [87] for further details. The possibility of such spurious contributions in two and three dimensions causes a complication for proposals to extract information about fracton topological orders from the scaling behavior of the entanglement entropy [103–105].

It would be interesting to explore the implications of compactification for decoding fracton topological codes [29,30]. While this may not be particularly useful for type-I models [106], since type-II models remain topological codes under compactification one may be able to apply techniques based on the 2D toric code. In particular, it should be possible to correct errors that are nonlocal in one spatial direction.

Another apparent future direction is the study of compactification with different boundary conditions. Open boundary conditions are particularly appealing due to their practical relevance. It would also be interesting to study the anyons and symmetry defects found after compactification as linelike objects in the uncompactified model. We plan to explore these directions in future work.

Further examples of compactification

The Appendix contains numerical calculations of n_{L_z}, the number of copies of toric code, for a wide range of fracton stabilizer models that have been compactified in the three lattice directions. It is clear that the scaling of n_{L_z} for TQFT, foliated fracton, fractal, and type-II fracton, topological stabilizer models is qualitatively different. The sorting of these 3D topological stabilizers is discussed in detail in a forthcoming work [107]. Our results demonstrate that compactification can serve as a useful tool in the sorting and classification of fracton topological orders. In Ref. [107], we go beyond this to discuss the coarse sorting and classification of 3D topological stabilizer models using tools such as the deformability of logical operators and anticommuting logical operator pairs supported on different configurations.

ACKNOWLEDGMENTS

A.D. thanks Mengzhen Zhang and Guanyu Zhu for useful discussions. This work is supported by startup funds at Yale University (D.J.W. and M.C.) and the Alfred P. Sloan foundation (M.C.).

APPENDIX: COMPACTIFICATION OF FURTHER EXAMPLES

In this Appendix, we report our numerical calculations of the number of copies of toric code as a function of compactification radius along each axis. We consider a wide range of fracton stabilizer models. The number of toric codes is reported for the compactified model after all local symmetry-breaking degeneracy has been lifted by adding 2D local operators to the compactified Hamiltonian. The models are labeled CC0-17, which stands for cubic code 0-17 following the notation in Ref. [31] which differs slightly from Ref. [2]. We also consider the 3D toric code, labeled 3D TC; Chamon's model [1,17], labeled Chm; another model found by Castelnovo and Chamon [16] and also Yoshida [4], which we label Y; the X-cube model and checkerboard model [7], labeled XC and

TABLE II. Number of copies of toric code as a function of compactification radius L_z for compactification along $\hat{z}$.

L_z	CC1	CC2	CC3	CC4	CC5	CC6	CC7	CC8	CC9	CC10	HH-II
2	4	2	4	4	2	2	2	2	4	2	8
3	2	1	2	4	1	1	5	5	6	1	4
4	8	4	8	8	4	4	4	4	8	4	16
5	10	9	10	10	5	5	9	9	10	9	20
6	4	2	4	8	2	2	10	10	12	2	16
7	14	13	14	14	7	7	13	13	14	13	28
8	16	8	16	16	8	8	8	8	16	8	32
9	14	13	14	16	7	7	17	17	18	13	28
10	20	18	20	20	10	10	18	18	20	18	40

TABLE III. Number of copies of toric code as a function of compactification radius L_z for compactification along $\hat{z}$. The superscript $*$ denotes that CB* and HH-I* have been coarse grained by a factor of two.

L_z	3D TC	Chm	X-cube	CB*	HH-I*	CC0	CC11	CC12	CC13	CC14	CC15	CC16	CC17	Y
2	1	2	1	2	4	8	4	4	4	2	4	2	4	0
3	1	4	2	4	8	12	4	6	2	6	6	5	2	0
4	1	6	3	6	12	16	8	8	8	3	8	4	8	0
5	1	8	4	8	16	20	10	10	10	10	10	9	10	0
6	1	10	5	10	20	24	8	12	4	10	12	10	8	0
7	1	12	6	12	24	16	14	14	14	14	14	13	14	0
8	1	14	7	14	28	32	16	16	16	11	16	8	16	0
9	1	16	8	16	32	36	16	18	14	18	18	17	14	0
10	1	18	9	18	36	40	20	20	20	18	20	18	20	0

TABLE IV. Number of copies of toric code as a function of compactification radius L_y for compactification along $\hat{y}$.

L_y	CC1	CC2	CC3	CC4	CC5	CC6	CC7	CC8	CC9	CC10	HH-II
2	4	2	2	2	2	2	4	2	2	2	8
3	2	1	1	5	5	5	6	5	5	1	4
4	8	4	4	4	4	4	8	4	4	4	16
5	10	9	9	9	9	9	10	9	9	9	20
6	4	2	2	10	10	10	12	10	10	2	16
7	14	13	13	13	13	13	14	13	13	13	28
8	16	8	8	8	8	8	16	8	8	8	32
9	14	13	13	17	17	17	18	17	17	13	28
10	20	18	18	18	18	18	20	18	18	18	40

CB respectively; and finally the so-called type-I and II spin models in Ref. [108], labeled HH-I and HH-II respectively. We remark that the checkerboard model is local unitary equivalent to two copies of the X-cube model [77] and similarly the HH-I model is mapped to two copies of the checkerboard model by applying swap gates to half the sites. We also point out that HH-II has *not* been shown to be a type-II model.

In the tables below, we group the fracton models that have not (have) been previously shown to support a string operator, i.e., the first table contains the type-II models, and some that may be type-I, while the second contains TQFT and type-I models and so on. We show our results for compactification in the $\hat{z}$, $\hat{y}$, and $\hat{x}$ directions, respectively. The quantity L_i denotes the compactification radius, and the superscript $*$ denotes that CB* and HH-I* have been coarse grained by a factor of 2. Tables II and III show number of copies of Toric code compactification along $\hat{z}$, Tables IV and V, along $\hat{y}$ direction and tables VI and VII along $\hat{x}$ direction.

We observe that the scaling behavior of the number of toric codes in the compactified model is indicative of the model's type. For TQFT (3D TC), the number of 2D toric codes is constant. For foliated type-I fracton orders (Chm, XC, CB, HH-I), the number scales linearly. For type II and fractal type I [107] (CC0-17, HH-II, Y), there is at least one direction where the number fluctuates as it grows with the compactification radius.

TABLE V. Number of copies of toric code as a function of compactification radius L_y for compactification along $\hat{y}$. The superscript $*$ denotes that CB* and HH-I* have been coarse grained by a factor of two.

L_y	3D TC	Chm	X-cube	CB*	HH-I*	CC0	CC11	CC12	CC13	CC14	CC15	CC16	CC17	Y
2	1	2	1	2	4	8	4	2	4	2	4	2	4	0
3	1	4	2	4	8	12	4	5	4	3	6	5	2	2
4	1	6	3	6	12	16	8	4	8	4	8	4	8	0
5	1	8	4	8	16	20	10	9	10	9	10	9	10	4
6	1	10	5	10	20	24	8	10	8	6	12	10	4	4
7	1	12	6	12	24	16	14	13	14	13	14	13	14	6
8	1	14	7	14	28	32	16	8	16	8	16	8	16	3
9	1	16	8	16	32	36	16	17	16	15	18	17	14	8
10	1	18	9	18	36	40	20	18	20	18	20	18	20	8

TABLE VI. Number of copies of toric code as a function of compactification radius L_x for compactification along $\hat{x}$.

L_x	CC1	CC2	CC3	CC4	CC5	CC6	CC7	CC8	CC9	CC10	HH-II
2	4	4	2	2	2	4	2	2	2	2	8
3	2	2	1	3	5	2	5	5	5	1	4
4	8	8	4	4	4	8	4	4	4	4	16
5	10	10	9	9	9	10	9	9	9	9	20
6	4	4	2	6	10	4	10	10	10	2	16
7	14	14	13	13	13	14	13	13	13	13	28
8	16	16	8	8	8	16	8	8	8	8	32
9	14	14	13	15	17	14	17	17	17	13	28
10	20	20	18	18	18	20	18	18	18	18	40

TABLE VII. Number of copies of toric code as a function of compactification radius L_x for compactification along $\hat{x}$. The superscript $*$ denotes that CB* and HH-I* have been coarse grained by a factor of two.

L_x	3D TC	Chm	X-cube	CB*	HH-I*	CC0	CC11	CC12	CC13	CC14	CC15	CC16	CC17	Y
2	1	2	1	2	4	8	2	4	4	2	2	2	4	0
3	1	4	2	4	8	12	1	6	6	2	5	5	2	2
4	1	6	3	6	12	16	4	8	8	3	4	4	8	0
5	1	8	4	8	16	20	5	10	10	10	9	9	10	4
6	1	10	5	10	20	24	4	12	12	2	10	10	4	4
7	1	12	6	12	24	16	7	14	14	14	13	13	14	6
8	1	14	7	14	28	32	8	16	16	11	8	8	16	3
9	1	16	8	16	32	36	7	18	18	14	17	17	14	8
10	1	18	9	18	36	40	10	20	20	18	18	18	20	8

[1] C. Chamon, Quantum Glassiness in Strongly Correlated Clean Systems: An Example of Topological Overprotection, Phys. Rev. Lett. **94**, 040402 (2005).

[2] J. Haah, Local stabilizer codes in three dimensions without string logical operators, Phys. Rev. A **83**, 042330 (2011).

[3] I. H. Kim, 3D local qupit quantum code without string logical operator, arXiv:1202.0052 (unpublished).

[4] B. Yoshida, Exotic topological order in fractal spin liquids, Phys. Rev. B **88**, 125122 (2013).

[5] J. Haah, Commuting Pauli Hamiltonians as maps between free modules, Commun. Math. Phys. **324**, 351 (2013).

[6] S. Vijay, J. Haah, and L. Fu, A new kind of topological quantum order: A dimensional hierarchy of quasiparticles built from stationary excitations, Phys. Rev. B **92**, 235136 (2015).

[7] S. Vijay, J. Haah, and L. Fu, Fracton topological order, generalized lattice gauge theory, and duality, Phys. Rev. B **94**, 235157 (2016).

[8] D. J. Williamson, Fractal symmetries: Ungauging the cubic code, Phys. Rev. B **94**, 155128 (2016).

[9] I. H. Kim and J. Haah, Localization from Superselection Rules in Translation Invariant Systems, Phys. Rev. Lett. **116**, 027202 (2016).

[10] A. Prem, J. Haah, and R. Nandkishore, Glassy quantum dynamics in translation invariant fracton models, Phys. Rev. B **95**, 155133 (2017).

[11] Y. You, T. Devakul, F. J. Burnell, and S. L. Sondhi, Symmetric fracton matter: Twisted and enriched, arXiv:1805.09800 (unpublished).

[12] A. T. Schmitz, H. Ma, R. M. Nandkishore, and S. A. Parameswaran, Recoverable information and emergent conservation laws in fracton stabilizer codes, Phys. Rev. B **97**, 134426 (2018).

[13] A. T. Schmitz, S.-J. Huang, and A. Prem, Entanglement spectra of stabilizer codes: A window into gapped quantum phases of matter, Phys. Rev. B **99**, 205109 (2019).

[14] S. Bravyi, M. B. Hastings, and S. Michalakis, Topological quantum order: Stability under local perturbations, J. Math. Phys. **51**, 093512 (2010).

[15] C. Castelnovo, C. Chamon, and D. Sherrington, Quantum mechanical and information theoretic view on classical glass transitions, Phys. Rev. B **81**, 184303 (2010).

[16] C. Castelnovo and C. Chamon, Topological quantum glassiness, Philos. Mag. **92**, 304 (2012).

[17] S. Bravyi, B. Leemhuis, and B. M. Terhal, Topological order in an exactly solvable 3D spin model, Ann. Phys. **326**, 839 (2010).

[18] H. Ma, E. Lake, X. Chen, and M. Hermele, Fracton topological order via coupled layers, Phys. Rev. B **95**, 245126 (2017).

[19] S. Vijay, Isotropic layer construction and phase diagram for fracton topological phases, arXiv:1701.00762 (unpublished).

[20] S. Vijay and L. Fu, A generalization of non-Abelian anyons in three dimensions, arXiv:1706.07070 (unpublished).

[21] K. Slagle and Y. B. Kim, Fracton topological order from nearest-neighbor two-spin interactions and dualities, Phys. Rev. B **96**, 165106 (2017).

[22] G. B. Halász, T. H. Hsieh, and L. Balents, Fracton Topological Phases from Strongly Coupled Spin Chains, Phys. Rev. Lett. **119**, 257202 (2017).

[23] T. Devakul, $Z3$ topological order in the face-centered-cubic quantum plaquette model, Phys. Rev. B **97**, 155111 (2018).

[24] T. Devakul, S. A. Parameswaran, and S. L. Sondhi, Correlation function diagnostics for type-I fracton phases, Phys. Rev. B **97**, 041110(R) (2018).

[25] A. Prem, S.-J. Huang, H. Song, and M. Hermele, Cage-Net Fracton Models, Phys. Rev. X **9**, 021010 (2019).

[26] D. Bulmash and T. Iadecola, Braiding and gapped boundaries in fracton topological phases, Phys. Rev. B **99**, 125132 (2019).

[27] H. Song, A. Prem, S.-J. Huang, and M. A. Martin-Delgado, Twisted fracton models in three dimensions, Phys. Rev. B **99**, 155118 (2019).

[28] Z. Weinstein, E. Cobanera, G. Ortiz, and Z. Nussinov, Absence of finite temperature phase transitions in the X-cube model and its $\mathbb{Z}_p$ generalization, arXiv:1812.04561.

[29] S. Bravyi and J. Haah, Energy Landscape of 3D Spin Hamiltonians with Topological Order, Phys. Rev. Lett. **107**, 150504 (2011).

[30] S. Bravyi and J. Haah, Quantum Self-Correction in the 3D Cubic Code Model, Phys. Rev. Lett. **111**, 200501 (2013).

[31] J. Haah, Lattice quantum codes and exotic topological phases of matter, arXiv:1305.6973 (unpublished).

[32] J. Haah, Bifurcation in entanglement renormalization group flow of a gapped spin model, Phys. Rev. B **89**, 075119 (2014).

[33] M. Pretko, Subdimensional particle structure of higher rank $U(1)$ spin liquids, Phys. Rev. B **95**, 115139 (2017).

[34] M. Pretko, Generalized electromagnetism of subdimensional particles: A spin liquid story, Phys. Rev. B **96**, 035119 (2017).

[35] M. Pretko, Emergent gravity of fractons: Mach's principle revisited, Phys. Rev. D **96**, 024051 (2017).

[36] M. Pretko, Higher-spin Witten effect and two-dimensional fracton phases, Phys. Rev. B **96**, 125151 (2017).

[37] M. Pretko, Finite-temperature screening of $U(1)$ fractons, Phys. Rev. B **96**, 115102 (2017).

[38] A. Prem, M. Pretko, and R. M. Nandkishore, Emergent phases of fractonic matter, Phys. Rev. B **97**, 085116 (2018).

[39] A. Prem, S. Vijay, Y. Z. Chou, M. Pretko, and R. M. Nandkishore, Pinch point singularities of tensor spin liquids, Phys. Rev. B **98**, 165140 (2018).

[40] S. Pai and M. Pretko, Fractonic line excitations: An inroad from three-dimensional elasticity theory, Phys. Rev. B **97**, 235102 (2018).

[41] M. Pretko and L. Radzihovsky, Fracton-Elasticity Duality, Phys. Rev. Lett. **120**, 195301 (2018).

[42] M. Pretko and L. Radzihovsky, Symmetry Enriched Fracton Phases from Supersolid Duality, Phys. Rev. Lett. **121**, 235301 (2018).

[43] M. Pretko, The fracton gauge principle, Phys. Rev. B **98**, 115134 (2018).

[44] K. Slagle, A. Prem, and M. Pretko, Symmetric tensor gauge theories on curved spaces, arXiv:1807.00827 (unpublished).

[45] A. Gromov, Fractional Topological Elasticity and Fracton Order, Phys. Rev. Lett. **122**, 076403 (2019).

[46] H. Ma, M. Hermele, and X. Chen, Fracton topological order from the Higgs and partial-confinement mechanisms of rank-two gauge theory, Phys. Rev. B **98**, 035111 (2018).

[47] D. Bulmash and M. Barkeshli, Higgs mechanism in higher-rank symmetric $U(1)$ gauge theories, Phys. Rev. B **97**, 235112 (2018).

[48] D. Bulmash and M. Barkeshli, Generalized $U(1)$ gauge field theories and fractal dynamics, arXiv:1806.01855 (unpublished).

[49] D. J. Williamson, Z. Bi, and M. Cheng, Fractonic matter in symmetry-enriched $U(1)$ gauge theory, arXiv:1809.10275 (unpublished).

[50] A. Gromov, Towards classification of Fracton phases: The multipole algebra, arXiv:1812.05104v1 (unpublished).

[51] R. M. Nandkishore and M. Hermele, Fractons, Ann. Rev. Conden. Matter Phys. **10**, 295 (2019).

[52] R. Dijkgraaf and E. Witten, Topological gauge theories and group cohomology, Commun. Math. Phys. **129**, 393 (1990).

[53] D. N. Yetter, TQFTs from homotopy 2-types, J. Knot Theory Ramifications **02**, 113 (1993).

[54] L. Crane and D. Yetter, in *Quantum Topology* (World Scientific, Singapore, 1993), pp. 1–11.

[55] L. Crane and I. B. Frenkel, Four-dimensional topological quantum field theory, Hopf categories, and the canonical bases, J. Math. Phys. **35**, 5136 (1994).

[56] J. Scott Carter, L. H. Kauffman, and M. Saito, Structures and diagrammatics of four dimensional topological lattice field theories, Adv. Math. **146**, 39 (1999).

[57] K. Walker and Z. Wang, (3+1)-TQFTs and topological insulators, Front. Phys. **7**, 150 (2012).

[58] A. Kapustin and R. Thorngren, Higher symmetry and gapped phases of gauge theories, Progr. Math. **324**, 177 (2017).

[59] S. X. Cui, Higher categories and topological quantum field theories Ph.D. thesis, University of California, Santa Barbara 2016, arXiv:1610.07628.

[60] D. J. Williamson and Z. Wang, Hamiltonian models for topological phases of matter in three spatial dimensions, Ann. Phys. **377**, 311 (2017).

[61] M. Bärenz and J. Barrett, Dichromatic state sum models for four manifolds from pivotal functors, Commun. Math. Phys. **360**, 663 (2018).

[62] A. Bullivant, M. Calçada, Z. Kádár, P. Martin, and J. F. Martins, Topological phases from higher gauge symmetry in 3+1 dimensions, Phys. Rev. B **95**, 155118 (2017).

[63] C. Delcamp and A. Tiwari, From gauge to higher gauge models of topological phases, J. High Energy Phys. 10 (2018) 049.

[64] S. Jiang, A. Mesaros, and Y. Ran, Generalized Modular Transformations in (3+1)D Topologically Ordered Phases and Triple Linking Invariant of Loop Braiding, Phys. Rev. X **4**, 31048 (2014).

[65] J. C. Wang and X. G. Wen, Non-Abelian string and particle braiding in topological order: Modular SL(3, Z) representation and (3+1)-dimensional twisted gauge theory, Phys. Rev. B **91**, 035134 (2015).

[66] C. Wang and M. Levin, Braiding Statistics of Loop Excitations in Three Dimensions, Phys. Rev. Lett. **113**, 080403 (2014).

[67] C. Wang and M. Levin, Topological invariants for gauge theories and symmetry-protected topological phases, Phys. Rev. B **91**, 165119 (2015).

[68] C. Y. Huang, X. Chen, and F. Pollmann, Detection of symmetry-enriched topological phases, Phys. Rev. B **90**, 045142 (2014).

[69] M. P. Zaletel, Y.-M. Lu, and A. Vishwanath, Measuring space-group symmetry fractionalization in $Z2$ spin liquids, Phys. Rev. B **96**, 195164 (2017).

[70] M. Barkeshli, P. Bonderson, C.-M. Jian, M. Cheng, and K. Walker, Reflection and time reversal symmetry enriched topological phases of matter: Path integrals, non-orientable manifolds, and anomalies, arXiv:1612.07792 (unpublished).

[71] K. Slagle and Y. B. Kim, X-cube model on generic lattices: Fracton phases and geometric order, Phys. Rev. B **97**, 165106 (2018).

[72] K. Slagle and Y. B. Kim, Quantum field theory of X-cube fracton topological order and robust degeneracy from geometry, Phys. Rev. B **96**, 195139 (2017).

[73] W. Shirley, K. Slagle, Z. Wang, and X. Chen, Fracton Models on General Three-Dimensional Manifolds, Phys. Rev. X **8**, 031051 (2018).

[74] W. Shirley, K. Slagle, and X. Chen, Foliated fracton order from gauging subsystem symmetries, SciPost Phys. **6**, 041 (2019).

[75] W. Shirley, K. Slagle, and X. Chen, Fractional excitations in foliated fracton phases, arXiv:1806.08625 (unpublished).

[76] W. Shirley, K. Slagle, and X. Chen, Universal entanglement signatures of foliated fracton phases, SciPost Phys. **6**, 015 (2019).

[77] W. Shirley, K. Slagle, and X. Chen, Foliated fracton order in the checkerboard model, Phys. Rev. B **99**, 115123 (2019).

[78] K. Slagle, D. Aasen, and D. Williamson, Foliated field theory and string-membrane-net condensation picture of fracton prder, SciPost Phys. **6**, 043 (2019).

[79] K. T. Tian, E. Samperton, and Z. Wang, Haah codes on general three manifolds, arXiv:1812.02101 (unpublished).

[80] Y. You, T. Devakul, F. J. Burnell, and S. L. Sondhi, Subsystem symmetry protected topological order, Phys. Rev. B **98**, 035112 (2018).

[81] T. Devakul, D. J. Williamson, and Y. You, Classification of subsystem symmetry-protected topological phases, Phys. Rev. B **98**, 235121 (2018).

[82] T. Devakul, Y. You, F. J. Burnell, and S. L. Sondhi, Fractal symmetric phases of matter, SciPost Phys. **6**, 007 (2019).

[83] T. Devakul and D. J. Williamson, Universal quantum computation using fractal symmetry-protected cluster phases, Phys. Rev. A **98**, 022332 (2018).

[84] A. Kubica and B. Yoshida, Ungauging quantum error-correcting codes, arXiv:1805.01836 (unpublished).

[85] S. Bravyi (unpublished).

[86] L. Zou and J. Haah, Spurious long-range entanglement and replica correlation length, Phys. Rev. B **94**, 075151 (2016).

[87] D. J. Williamson, A. Dua, and M. Cheng, Spurious Topological Entanglement Entropy from Subsystem Symmetries, Phys. Rev. Lett. **122**, 140506 (2019).

[88] G. Moore and N. Seiberg, Classical and quantum conformal field theory, Commun. Math. Phys. **123**, 177 (1989).

[89] K. Alexei, Anyons in an exactly solved model and beyond, Ann. Phys. **321**, 2 (2006).

[90] H. Bombín, Structure of 2D topological stabilizer codes, Commun. Math. Phys. **327**, 387 (2014).

[91] J. Haah, Algebraic methods for quantum codes on lattices, Revista Colombiana de Matemáticas **50**, 299 (2016).

[92] J. Haah, Classification of translation invariant topological Pauli stabilizer codes for prime dimensional qudits on two-dimensional lattices, arXiv:1812.11193 (unpublished).

[93] A. R. Calderbank and P. W. Shor, Good quantum error-correcting codes exist, Phys. Rev. A **54**, 1098 (1996).

[94] A. Steane, Multiple-particle interference and quantum error correction, Proc. R. Soc. A **452**, 2551 (1996).

[95] A. Y. Kitaev, Fault-tolerant quantum computation by anyons, Ann. Phys. **303**, 2 (2003).

[96] J. Haah, An invariant of topologically ordered states under local unitary transformations, Commun. Math. Phys. **342**, 771 (2016).

[97] J. C. Bridgeman, S. T. Flammia, and D. Poulin, Detecting topological order with ribbon operators, Phys. Rev. B **94**, 205123 (2016).

[98] A. Kitaev and J. Preskill, Topological Entanglement Entropy, Phys. Rev. Lett. **96**, 110404 (2006).

[99] M. Barkeshli, P. Bonderson, M. Cheng, and Z. Wang, Symmetry, defects, and gauging of topological phases, arXiv:1410.4540 (unpublished).

[100] D. Eisenbud, *Commutative Algebra with a View Toward Algebraic Geometry*, 1st ed., Graduate Texts in Mathematics Vol. 150 (Springer-Verlag, New York, 2004).

[101] S. Lang, *Algebra* (Springer-Verlag, New York, 2002).

[102] M. Levin and X. G. Wen, Detecting Topological Order in a Ground State Wave Function, Phys. Rev. Lett. **96**, 110405 (2006).

[103] B. Shi and Y. M. Lu, Deciphering the nonlocal entanglement entropy of fracton topological orders, Phys. Rev. B **97**, 144106 (2018).

[104] H. Ma, A. T. Schmitz, S. A. Parameswaran, M. Hermele, and R. M. Nandkishore, Topological entanglement entropy of fracton stabilizer codes, Phys. Rev. B **97**, 125101 (2018).

[105] H. He, Y. Zheng, B. A. Bernevig, and N. Regnault, Entanglement entropy from tensor network states for stabilizer codes, Phys. Rev. B **97**, 125102 (2018).

[106] B. J. Brown and D. J. Williamson, Parallelized quantum error correction with fracton topological codes, arXiv:1901.08061 (unpublished).

[107] A. Dua, D. J. Williamson, and M. Cheng, Towards classification of topological stabilizer models in 3d (unpublished).

[108] T. H. Hsieh and G. B. Halász, Fractons from partons, Phys. Rev. B **96**, 165105 (2017).